CRYSTAL GROWTH & DESIGN

pubs.acs.org/crystal

Article

Polymorph-Selective Role of Hydrogen Bonding and $\pi-\pi$ Stacking in *p*-Aminobenzoic Acid Solutions

Raitis Bobrovs,* Laura Drunka, Andrievs Auseklis Auzins, Kristaps Jaudzems, and Matteo Salvalaglio*

Cite This: https://dx.doi.org/10.1021/acs.cgd.0c01257

Read Online

ACCESS | Metrics & More | Article Recommendations | Supporting Information

ABSTRACT: Understanding molecular self-association in solution is vital for uncovering polymorph-selective crystal nucleation pathways. In this paper, we combine solution NMR spectroscopy and molecular dynamics simulations to shed light on the structural and dynamical features of *p*-aminobenzoic acid (pABA) in solution, and on their role in pABA crystals nucleation. pABA is known to yield different crystal forms (α, and β) depending on solvent choice and supersaturation conditions. NMR reveals that dominant interactions stabilizing pABA oligomers are markedly solvent-dependent: in organic solvents, hydrogen bonds dominate, while water promotes $\pi-\pi$ stacking. Despite this clear preference, both types of interactions contribute to the variety of self-associated species in all solvents considered. MD simulations support this observation and show that pABA oligomers are short-lived and display a fluxional character, therefore indicating that the growth unit involved in pABA crystallization is likely to be a single molecule. Nevertheless, we note that the interactions dominating in pABA oligomers are indicative of the polymorph obtained from precipitation. In water, at low pABA concentrations—conditions that are known to yield crystals of the β form—carboxylic−carboxylic hydrogen bonds are exclusively asymmetric. At higher pABA concentration conditions in which the crystallization is known to yield the α form—a small but statistically significant fraction of symmetric carboxylic−carboxylic hydrogen-bonded dimers is present. We interpret the presence of these interactions in solvated pABA oligomers as indicative of the fact that a simultaneous and complete desolvation of two carboxylic groups, necessary to form the symmetric hydrogen-bonded dimer typical of the α crystal form, is accessible, therefore directing the nucleation pathway toward the nucleation of α-pABA.

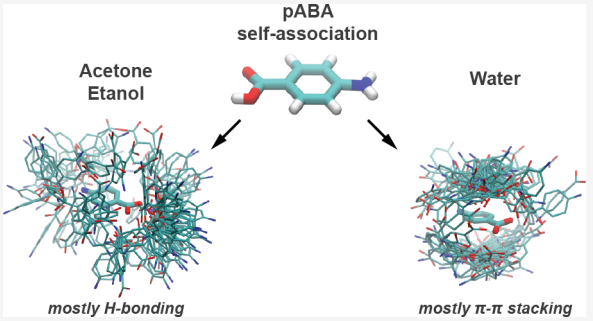

INTRODUCTION

Crystallization is by far the most popular separation and purification method employed to produce a wide range of materials in the chemical, food, and pharmaceutical industries.[1] Nevertheless, the detailed mechanisms responsible for crystal nucleation are still largely unclear.[2,3] Alongside understanding the properties of bulk crystalline phases, in order to advance our understanding of crystal formation pathways, it is important to rationalize the structure and dynamics of processes taking place in the metastable phases where crystals are born.

The self-association of solute molecules in complexes with specific coordination stoichiometry, geometry, and solvation structure plays a central role in determining nucleation pathways, especially in polymorphic systems—which can crystallize in more than one phase.[1−3]

It is well-known that the outcome of crystallization in polymorphic systems is affected by solvent choice, solute concentration, temperature, pressure, etc.[1,4,5] All these variables affect the solute self-association and, in turn, impact nucleation mechanisms at the molecular scale. It is precisely at this scale that our knowledge of nucleation is still rather poor due to the lack of methods that simultaneously provide appropriate spatial and temporal resolution. Techniques that have been successfully used to widen our understanding on initial molecule self-association and nucleation include small/wide-angle X-ray scattering (SAXS/WAXS),[6−11] cryogenic transmission electron microscopy (cryo-TEM),[11−20] atomic electron tomography (AET),[21] nuclear magnetic resonance (NMR),[22−36] Fourier-transform infrared and ultraviolet (FTIR/UV−vis)[36−43] spectroscopy, and ever increasingly molecular dynamics (MD) simulations.[44−61] However, each of these methods has its limitations, and in order to gain in-depth knowledge on crystal nucleation, the combination of several methods in the same framework is highly desirable.

pABA Polymorphs. pABA is known to exist in four different polymorphic forms—α, β, γ,[62] and δ.[63] Here we focus on the nucleation of the two forms of pABA that can be

Received: September 11, 2020
Revised: November 19, 2020

produced at ambient conditions by varying the composition of the mother phase, namely the α and β forms (Figure 1). Form

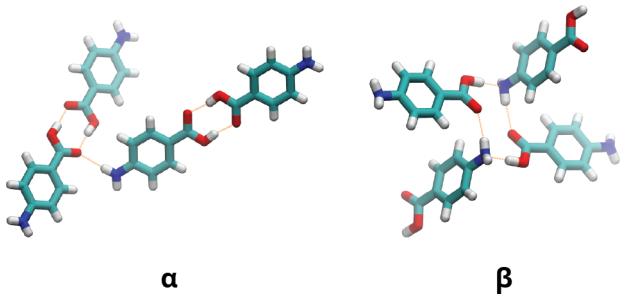

Figure 1. Crystal packing motifs in *p*-aminobenzoic acid α and β forms. Hydrogen bonds are indicated with orange dashed lines.

α is the most accessible polymorph, as it can be produced by crystallizing from nearly all solvents and supersaturations.[64] The β polymorph can only be consistently obtained by crystallization from water or ethyl acetate under careful control of supersaturation ($\lesssim$1.35) and temperature or by solvent-mediated phase transformation below the polymorph equilibrium temperature of 14 °C.[64−66] Interestingly, the temperature does not affect crystallization outcome from water, implying that crystallization of pABA does not follow Ostwald's rule of stages,[67,68] and the crystalline phase obtained is determined solely by supersaturation. Both forms seem to have comparable stability, as no phase transformations between α and β polymorph are observed over the 24 h period in the temperature range 5−26 °C.[67] This observation indicates that the crystalline phase obtained in crystallization experiments reflects the primary nucleation process, and it is not a result of rapid transformation from a metastable phase intermediate. Polymorphism of pABA has been recently discussed in-depth by Cruz-Cabeza et al.[69]

pABA Solution Chemistry. While most of the studies agree that pABA molecules in solution exist in some aggregated form, there is no consensus on the characteristics of the dominant self-associates. A seminal work by Gracin at al.[64] reached the conclusion that pABA solutions have a tendency to form *hydrogen-bonded carboxylic dimers*, especially in solvents of lower polarity. The findings of follow-up studies[65] expanded on this idea, implying that the pre-existence of dimers in solution facilitates the formation of the dimer-based α form. An extensive, multitechnique study by Toroz et al.[10] on pABA nucleation from ethanol solution also reported that the dominant species in solution are hydrogen-bonded carboxylic dimers.

On the other hand, solid-state and solution FTIR studies of saturated solutions of pABA in acetonitrile, 2-propanol, and ethyl acetate[42] led to the conclusion that pABA molecules exist *mostly as monomers* (with a small fraction of weakly self-associated pABA molecules), and solution composition does not change with concentration. These findings suggest that the growth of α form nuclei mostly occurs through $\pi-\pi$ stacking (in the [010] direction), whereas the rate-limiting step in crystal growth is desolvation of the carboxylic acid groups.

Studies of structurally related benzoic acid in methanol solution[70] indicated that solute−solute interactions are dominated by a combination of $\pi-\pi$ *stacking* (*face-to-face*, *T-shaped*) and *carboxylic−aromatic proton interactions*. The existence of cyclic hydrogen-bonded dimer as a major feature in methanol solution was rejected, and it was hypothesized that any solute−solute hydrogen-bonded interactions in methanol are closer in concept to a *catemeric motif* than a dimer. Subsequent nucleation induction time studies[71] in various benzoic acid solutions support the idea that crystal nucleation rate is determined by the rate of cluster growth, which in turn is controlled by the attachment of molecules to the nucleus via aromatic stacking.

Recently, Cruz-Cabeza et al.[72] explored the possible β pABA nucleation pathways using CSD data mining, crystal structure prediction, and targeted crystallizations; however, no convincing evidence for any form of self-associates, involving solute and/or solvent, that might be considered as a transition state in the nucleation of β pABA was reached. Their studies led to the conclusion that β pABA nucleation from water at low supersaturation is a result of local nucleation and growth *dead zone*, created by unusually high pABA/water interfacial tension, where α clusters cannot grow, thus giving time for a β form to appear.

With this work, we contribute to the debate on pABA crystallization by developing a dynamical description of pABA self-associates speciation in solution. To this aim, we combine NMR spectroscopy and molecular dynamics (MD) simulations in explicit solvent, two techniques that allow us to directly draw information on the structure of the liquid phase at finite temperature conditions. While NMR provides experimental evidence of the nature of pABA−pABA intermolecular interactions dominating in the liquid phase, MD enables one to determine the finite-temperature equilibrium distribution of self-associates, their abundance relative to monomers, and their characteristic lifetime. These approaches provide a rationale for the polymorph-selective role played by solvent and supersaturation in the crystallization of pABA.

RESULTS AND DISCUSSION

We studied pABA self-association in 3 different solvents—water, ethanol, and acetone. Water was selected due to its ability to facilitate nucleation of the reluctant β form at low supersaturation, whereas ethanol and acetone were selected as examples of solvents that lead to the precipitation of α form crystals. While NMR can be used to gain information on solute self-association in solution, it does not provide any direct information on their molecular arrangement. NMR spectroscopy was used to gain indirect information on the structure of aggregates by comparing pABA with tailored reference systems. NMR studies were complemented by MD simulations in which the equilibrium population of self-associated aggregates was quantitatively characterized.

NMR Experiments. It is generally recognized that the fraction of self-associated molecules in solution is affected by solution concentration. Higher concentrations induce the formation of self-associated adducts including dimers, trimers, and larger aggregates. The formation of self-associates changes the local electromagnetic environment of the nuclei that are involved in the interactions responsible for their stabilization or are in close proximity to those involved, therefore enabling a systematic study of self-association using NMR spectroscopy. Changes in the NMR chemical shifts as a function of solution concentration have been used in numerous studies[22,23,31,32,34−36,73] to characterize solute self-association in solution. In most cases, the hydrogen bonding induced by an increase in solute concentration leads to a displacement of the ^{1}H chemical shift to lower fields due to proton deshielding.

https://dx.doi.org/10.1021/acs.cgd.0c01257
Cryst. Growth Des. XXXX, XXX, XXX−XXX

Involvement in hydrogen bonding weakens covalent bonds involving hydrogen, leading to an increase in the average bond length, and hence to a decrease in the characteristic bond stretching frequency. The carboxylic and amino group protons take part in the proton exchange with the deuterium atoms of the solvent used in NMR experiments. As a result these protons are not "visible" in the NMR spectrum. Nevertheless, the ^{13}C NMR spectroscopy is not affected by proton exchange, and therefore, it can be used as an indicator of the interactions involving the carboxylic group. Due to this reason, we chose the ^{13}C NMR spectroscopy for our studies.

To determine experimentally whether the $\pi-\pi$ stacking or hydrogen bonding dominates in pABA complexes formed in water, ethanol, and acetone solutions, we studied reference systems that allow decoupling the contribution of these interactions to chemical shifts. Information about the dominant interactions in pABA solutions was then determined by comparing NMR chemical shift changes upon dilution between pABA and reference systems tailored to highlight the effect of specific moieties. Molecules of similar size and structure to pABA were selected as reference systems (Figure 2).

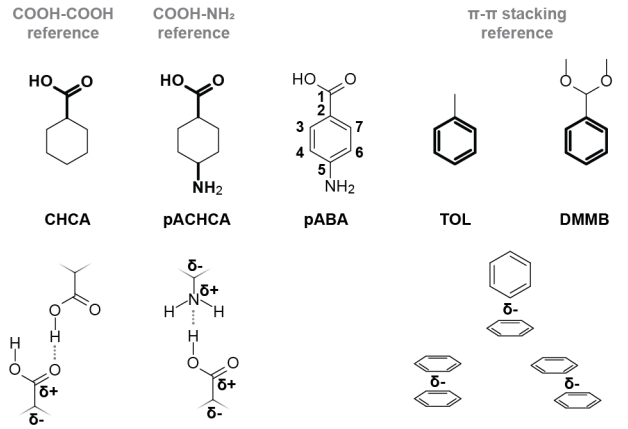

Figure 2. Top: Molecular structures of *p*-aminobenzoic acid (pABA) and reference compounds with respective abbreviations used in this study. Atom numbering scheme is indicated for pABA and was the same for all the reference compounds. Bottom: Expected changes in atom partial charges upon self-association.

Cyclohexane carboxylic acid (**CHCA**) was chosen as a reference for carboxylic−carboxylic hydrogen bonding, whereas the impact of $\pi-\pi$ stacking on associates formation was evaluated by examining trends associated with the dilution of toluene (**TOL**) and (dimethoxymethyl)benzene (**DMMB**) solutions. Finally, *p*-aminocyclohexane carboxylic acid (**pACHCA**), which exists in zwitterionic form at neutral pH in the solvents studied, allowed us to probe the hydrogen bonding between the carboxylic and amino moieties.

The concentration range studied was from 1 mol L^{-1} to 10 μmol L^{-1}. Such a concentration range was selected to cover the widest concentration region possible by performing the measurements within reasonable time frame. For systems where the desired upper concentration of 1 mol L^{-1} could not be achieved due to poor solubility, the range up to saturation concentration was covered.

Ethanol and Acetone Solutions. The ^{13}C NMR data indicate that hydrogen bonding dominates in pABA ethanol and acetone solutions. Increasing concentration displaces the ^{13}C chemical shift of the pABA carboxylic group carbon (C1, see Figure 2) toward lower fields, just like in the hydrogen bonding reference system **CHCA** (see Figure 3). The deshielding of the carboxylic group C1 with increasing concentration implies that electrons are withdrawn from the carboxylic group. The most likely cause for this effect is the involvement in carboxylic hydrogen bonding (Figure 2). The carbon right next to the carboxylic group (C2) also exhibits noticeable changes in the ^{13}C chemical shift upon concentration changes. C2 shielding increases with concentration due to electrons being drawn toward the carboxylic group upon hydrogen bonding. This effect is particularly pronounced in conjugated electron systems where the carboxylic group is right next to an aromatic system. This explains why there is rather minor C2 ^{13}C chemical shift displacement in **CHCA**, while in pABA C2 ^{13}C chemical shift displacement toward stronger fields reaches ∼0.5 ppm in acetone.

While qualitative ^{13}C chemical shift displacement patterns match for both organic solvents, several differences can be noticed. The ^{13}C chemical shift displacement for the C1 and C2 atoms in acetone is up to 1 order of magnitude larger than in ethanol. This could indicate either that the fraction of hydrogen-bonded pABA molecules in acetone is higher than in ethanol or, more likely, that the chemical shift displacement effect is more pronounced in acetone. For instance, in acetone, there are no labile protons that could interact with the carbonyl group of pABA, whereas the hydroxyl group in ethanol can form hydrogen bonds with the carboxylic group of pABA, therefore providing additional shielding for the C1 and C2 atoms. This additional shielding/deshielding effect is expected to be more pronounced upon dilution and is considered to account for the order-of-magnitude difference in ^{13}C chemical shift displacement. Similar differences between ethanol and acetone are observed in the chemical shift displacement profile for the carbon right next to the amino group (C5). This trend indicates that in ethanol the amino group becomes increasingly shielded with concentration, as the nitrogen-free electron pair interacts with the labile proton of ethanol. In contrast, in acetone, no additional shielding is observed. The ^{13}C chemical shift changes for the rest of the aromatic carbons are rather minor, indicating that local environment for these carbons is affected only slightly, as expected in carboxylic hydrogen-bonded dimers. The observed preference for the hydrogen bonding in acetone and ethanol is consistent with previous studies,[42] indicating that aprotic and weak hydrogen bond donor/acceptor solvents favor the formation of carboxylic dimers.

The ^{13}C chemical shift displacements in the $\pi-\pi$ stacking reference systems **TOL** and **DMMB** showed completely different patterns. In both references, chemical shifts for all carbon atoms are displaced toward higher fields as concentration increases. This pattern can be interpreted as the result of stacked $\pi-\pi$ electron systems providing additional shielding in the magnetic field due to the magnetic anisotropy of aromatic systems. It was not possible to record NMR spectra for **pACHCA** in organic solvents within a reasonable time due to poor solubility (**pACHCA** exists mostly in its zwitterionic form, that is insoluble in most organic solvents).

Given these observations, while it cannot be excluded that $\pi-\pi$ stacking contributes to the self-association in organic solvents, it is safe to conclude that in these systems carboxylic−carboxylic hydrogen bonding is dominant. The data obtained

https://dx.doi.org/10.1021/acs.cgd.0c01257
Cryst. Growth Des. XXXX, XXX, XXX−XXX

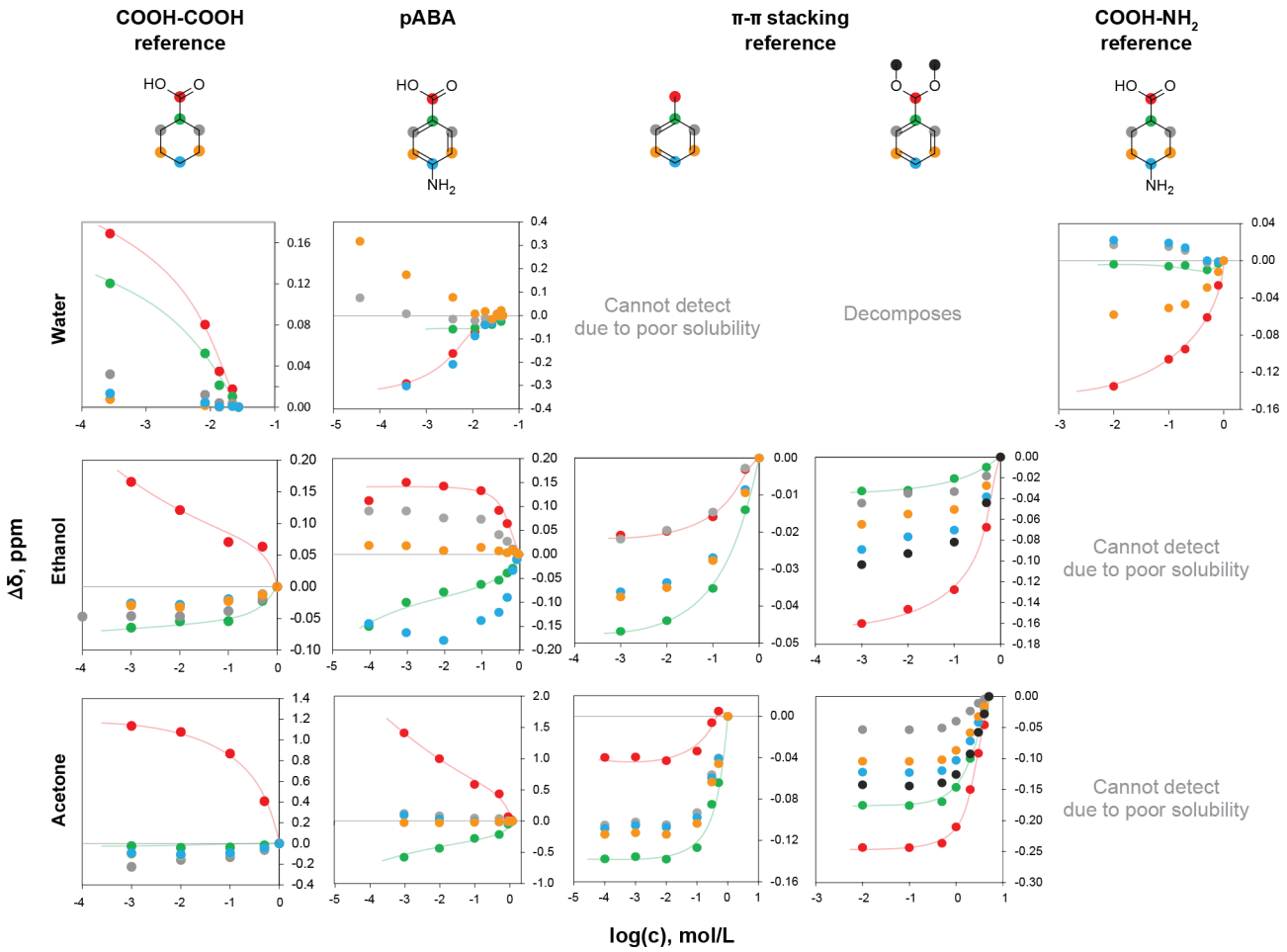

Figure 3. pABA and reference system ^{13}C chemical shift changes ($\Delta\delta$ with respect to the most concentrated solution) as a function of water, acetone, and ethanol solution concentrations. Lines for C1 and C2 chemical shift changes are added as a guide for the eye.

do not provide direct information on the structure of the H-bonded self-associates, and thus they cannot provide a distinction between symmetric hydrogen-bonded dimers or larger hydrogen-bonded associates (trimers, tetramers, catemers, etc.).

Water Solution. The pABA ^{13}C chemical shift displacement pattern in water is considerably different than in ethanol and acetone solutions. The carboxylic carbon C1 ^{13}C chemical shift is displaced to higher fields with increasing concentrations, indicating an increased shielding upon self-association. The most likely reason for such an observation would be $\pi-\pi$ stacking. Unfortunately, the ^{13}C chemical shift displacement pattern for both $\pi-\pi$ stacking reference systems in water could not be recorded due to poor **TOL** solubility and **DMMB** hydrolysis. Nevertheless, the comparison against $\pi-\pi$ reference systems in organic solvents partially supports this assumption. In Figure 3, it can be seen that chemical shift displacement patterns for C1 and C2 atoms in pABA follow the pattern traced by the analogous atoms in the $\pi-\pi$ reference systems in organic solvents. A difference in the concentration dependence of the chemical shifts between aromatic C4 and C6, and to a lesser extent C3 and C7, is observed, as these atoms are deshielded upon concentration increase. The data available do not provide a clear explanation about the ^{13}C chemical shift displacement pattern for these aromatic nuclei. Nevertheless, the existence of a pABA carboxylic−carboxylic hydrogen-bonded dimer as a dominant species in water results to be extremely unlikely, since in the carboxylic−carboxylic hydrogen bonding reference system **CHCA** all chemical shifts are displaced to lower fields with a concentration increase. The existence of carboxylic−amino hydrogen bonding seems to be more plausible. The carboxylic carbon C1 chemical shift displacement pattern in pABA follows the same pattern as C1 in **pACHCA**; however, the chemical shift displacement for the C5 right next to the amino group is completely different. In **pACHCA**, C5 becomes deshielded upon concentration increase, as expected upon hydrogen bonding, whereas in the pABA water solution the opposite trend is observed. However, here we need to keep in mind that due to the pABA conjugated electron system, electron withdrawal from the amino group upon hydrogen bonding should increase electron density on the C5. Besides, the amino group in pABA and nonzwitterionic **pACHCA** can act as hydrogen bond donor or acceptor, and it is not excluded that the preference for either hydrogen bond donating and accepting properties changes from one system to another, thus impacting the C5 chemical shift displacement pattern.

Overall, the ^{13}C chemical shift displacement pattern in pABA water solution suggests that, rather than being dominated by carboxylic−carboxylic hydrogen bonding, self-association in water solution is characterized by multiple interacting motifs. Within this picture, $\pi-\pi$ stacking and carboxylic−amino group hydrogen bonding emerge as the most prominent interactions.

https://dx.doi.org/10.1021/acs.cgd.0c01257
Cryst. Growth Des. XXXX, XXX, XXX−XXX

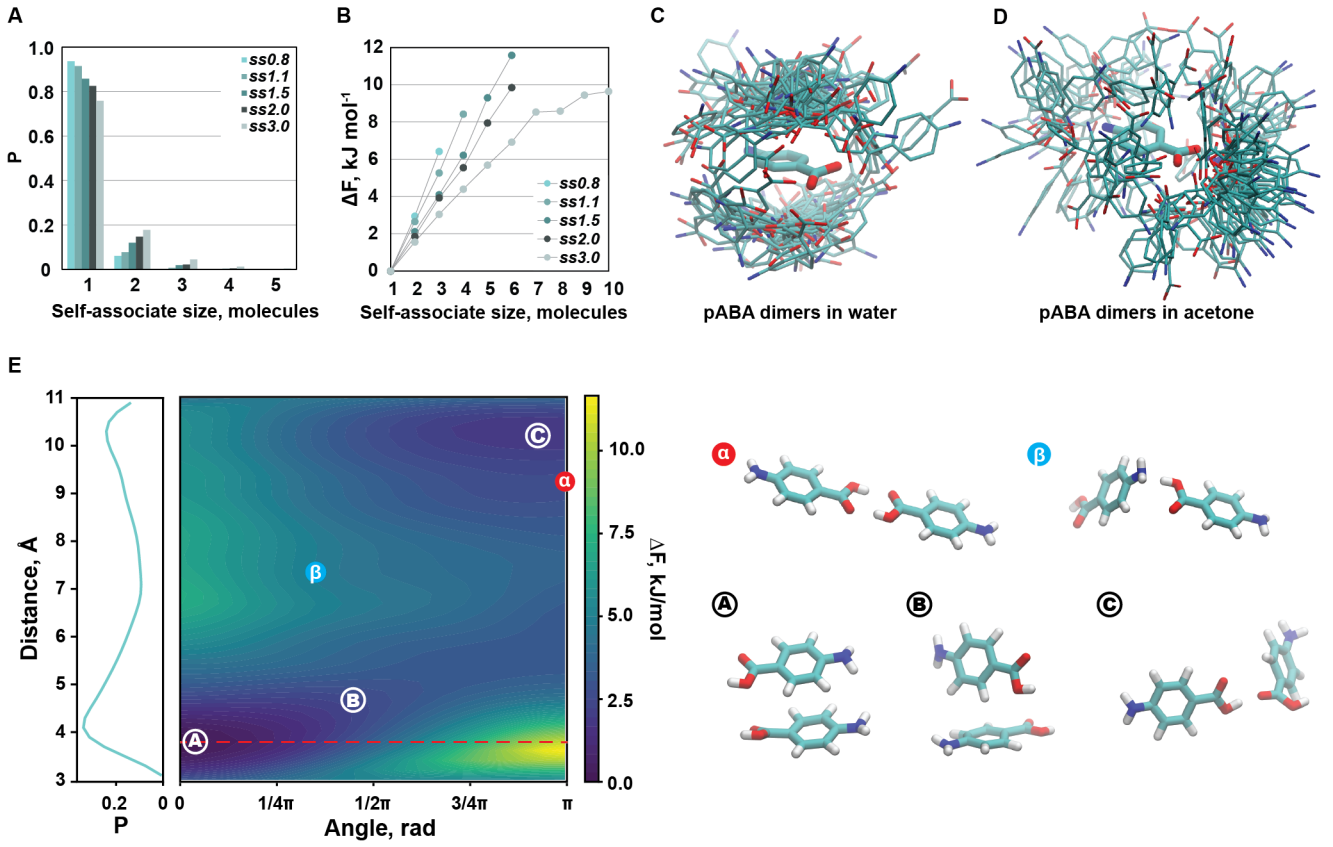

Figure 4. (A) Probability for the pABA molecule to be part of the self-associate of a specific size. (B) Energetic penalty associated with the formation of the self-associate of a specific size. An example of pABA molecule relative position in self-associated aggregates in water (C) and acetone (D) solutions. 100 randomly selected pABA dimers are shown; one pABA molecule of the dimer is superimposed (thick sticks). (E) Free energy profile of self-associated pABA dimers in water solution *ss1.1* as a function of intermolecular pABA distance and relative orientation. Red dashed line represents intermolecular distance in *face-to-face*π—π stacked dimers. A red circle indicates location of α form dimer on the FES; blue shows the β form.

Table 1. Fraction of pABA Molecules Involved in π–π Stacked and Hydrogen-Bonded Aggregate Formation, Lifetime of These Aggregates, and Distribution into Specific Aggregate Subtypes

		π–π stacked aggregates						hydrogen-bonded aggregates				
				fraction of all π–π stacking interactions						fraction of all hydrogen bonding interactions		
solvent	ss	fraction from total	lifetime, ps	*face-to-face*	*T-shaped*	*offset*	*intermediate*	fraction from total	lifetme, ps	*COOH–COOH (symmetric)*	*COOH–NH$_2$*	*NH$_2$–NH$_2$*
water	0.8	5.9	87.9	1.78	16.5	61.6	20.2	0.73	27.4	31.1 (0)	55.9	13.0
	1.1	8.0	80.5	1.74	18.2	56.6	23.5	0.92	27.3	27.8 (0)	58.6	13.5
	1.5	13.8	80.9	1.82	18.1	57.7	22.4	1.64	28.2	27.0 (0)	57.2	15.8
	2.0	17.0	81.2	1.70	18.0	58.4	21.9	1.96	30.1	25.7 (1.2)	60.1	14.2
	3.0	24.4	77.7	1.76	18.9	56.8	22.5	3.41	31.5	28.1 (1.7)	58.3	13.7
ethanol	0.8	16.8	46.9	0.51	49.1	25.9	24.5	46.1	81.6	45.3 (14.1)	44.6	10.1
	1.1	21.1	49.7	0.51	48.7	26.2	24.5	55.7	84.4	45.8 (13.0)	44.5	9.8
	1.5	35.6	55.5	0.51	48.0	26.9	24.6	86.4	91.5	44.1 (12.5)	45.5	10.3
acetone	0.8	6.1	32.4	0.19	65.8	12.6	21.5	35.1	92.6	50.9 (22.5)	44.4	4.7
	1.1	7.9	33.2	0.21	65.6	12.7	21.5	44.0	92.6	50.5 (21.5)	44.5	5.0
	1.5	14.2	36.1	0.21	64.5	13.7	21.6	67.9	93.5	48.2 (20.0)	46.1	5.7

MD Simulations. While the NMR data on both pABA and reference systems provided information on the most likely interactions stabilizing pABA self-associates in solution, detailed information on the self-association process at a molecular scale was obtained from MD simulations. By implicitly including entropic, solvent, and dynamical effects, MD simulations complement the wealth of information based on static calculations extensively reported in the literature.[10,65,68,71,72,74−80] Solution concentrations for MD studies were selected to correspond to supersaturation values (ss) 0.8, 1.1 and 1.5, where *ss0.8* was selected as a representative example of under-saturated solutions, *ss1.1*, as a system that in water would lead to crystallization of the β form, and *ss1.5*, as a system that would lead to crystallization of α form in all

https://dx.doi.org/10.1021/acs.cgd.0c01257
Cryst. Growth Des. XXXX, XXX, XXX−XXX

solvents. Since the solubility of pABA in water is low, additional simulations at supersaturation 2.0 and 3.0 were performed in water, to ensure that self-association differences at low and high concentration are not missed due to small differences in the system composition. MD simulations of all the reference systems were also performed and analyzed according to the same protocols applied to pABA. The results emerging from MD simulations of reference systems confirm the expectations in term of relative abundance of specific interaction motifs. Detailed results for the reference systems are reported and commented on in the Supporting Information.

Water Solution. MD simulations of undersaturated and supersaturated pABA water solutions revealed that spontaneous pABA molecule self-association occurs in all systems. Nevertheless, the majority of pABA molecules in water solution were in the monomeric state (Figure 4A). The dominant aggregate species in water is the dimer, with a fraction of ∼7% of pABA molecules self-associated in undersaturated conditions (*ss0.8*), up to ∼28% in highly supersaturated conditions (*ss3.0*, see Table 1). The energetic penalty for pABA dimer formation was 2.9 kJ mol^{-1} for undersaturated system *ss0.8*, down to 1.6 kJ mol^{-1} for supersaturated system *ss3.0* (Figure 4B). Occasionally, pABA trimers and tetramers were also observed. As expected, the fraction of self-associated molecules as well as the fraction of larger self-associated complexes increases with concentration.

An analysis of the free energy surface (FES) as a function of distance and angle between self-associated pABA molecules, reported in Figure 4E, reveals that there are two types of aggregates in aqueous solution with one of them noticeably favored. The global energy minimum at a pABA−pABA intermolecular distance ∼4 Å corresponds to $\pi-\pi$ stacked dimers, and accounts for the coordination geometry of ∼90% of all the self-associated pABA in aqueous solution. The shallow, wide local minimum at a distance of ∼10 Å corresponds to pABA−pABA hydrogen-bonded associates.

Aromatic Interactions. The dominant type of aromatic interaction in water solution was *offset* $\pi-\pi$ *stacked dimer* (∼57%), which is believed to be the energetically most favored.[81,82] The fraction of *T-shaped dimers* in the solution was ∼18%, whereas *face-to-face* $\pi-\pi$ *stacked dimers* accounted only for ∼1.8% of all stacked dimers. The rest of the aromatic stacked dimers are arranged into intermediate[82] stacked structures (Table 1). The analysis reveals a minor preference for *head-to-head* and *head-to-tail* pABA relative orientations in *face-to-face* and *offset* π—π stacked dimers (Figure 5, top); nevertheless, the relative position and orientation of stacked pABA molecules was still rather stochastic (see Figure 4, parts C and D). In *T-shaped* dimers there was a distinct preference for both molecule vectors to be in parallel planes (Figure 5, bottom), and no phenyl ring interactions with either amino or carboxylic group were observed. Despite concentrations leading role in determining the total fraction of pABA molecules involved in aggregate formation, the relative probability of different pABA complexes was maintained across all concentrations studied. The lifetime of $\pi-\pi$ stacked pABA aggregates follows an exponential distribution with mean characteristic time of ∼80 ps (additional details on the calculation of the aggregates lifetime is discussed in the Supporting Information).

Hydrogen Bonding. The probability for pABA molecules to be hydrogen-bonded to other pABA molecule was found to

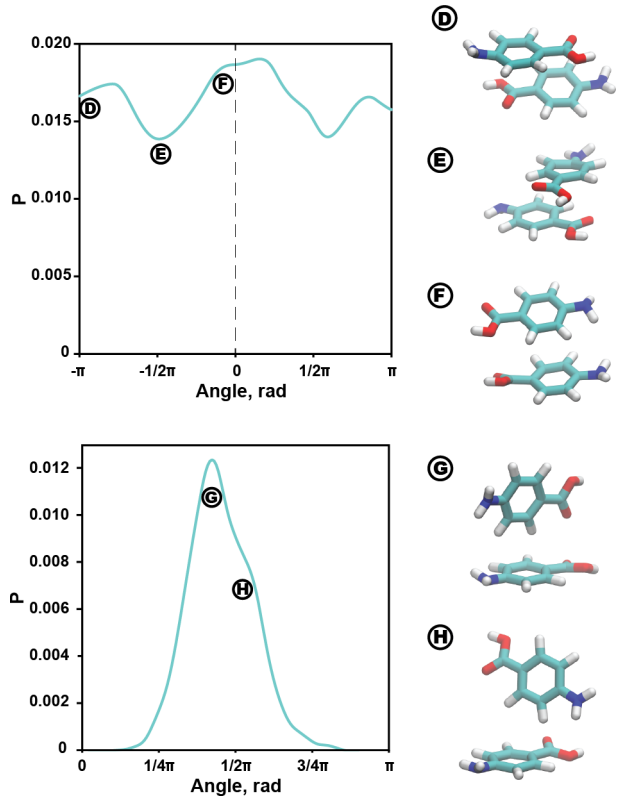

Figure 5. Top: Probability distribution of pABA molecule relative orientation in *face-to-face* and *offset* $\pi-\pi$ stacked dimers. Bottom: Probability distribution of pABA molecule relative orientation in *T-shaped* $\pi-\pi$ dimers. pABA dimer examples with their location indicated on the probability curves are given on the left.

range between 0.7% and 3.4% in water solutions (Table 1). Carboxylic−amino group hydrogen bonding was the preferred polar interaction recorded in aqueous solution, with ∼50% of all hydrogen-bonded dimers in which the amino group was the hydrogen bond donor and ∼7% of hydrogen bonds where the amino group was the hydrogen bond acceptor.

Hydrogen bonding between two amino groups accounted for ∼15% of all polar interactions. Carboxylic−carboxylic pABA hydrogen bonding, traditionally considered the dominant interaction in solution, accounted on average for ∼28% of all pABA−pABA hydrogen-bonded complexes. The relative probability of different hydrogen bonding types emerged as independent of concentration, with the notable exception of the relative proportion between symmetric and asymmetric carboxylic−carboxylic hydrogen bonds. In lower supersaturations (up to *ss1.5*) carboxylic−carboxylic hydrogen bonds were exclusively asymmetric, whereas, upon concentration increase, symmetric carboxylic−carboxylic hydrogen-bonded dimers were observed, accounting for up to 1.7% of all carboxylic−carboxylic dimers in highly supersaturated water solutions *ss3.0*. From the analysis of the equilibrium distribution of self-associated species, it emerges that the experimentally known dependence of the polymorphic outcome of pABA crystallization from aqueous solutions correlates with the observation of an increase in symmetrical carboxyl−carboxyl hydrogen-bonded dimers. For instance, the low supersaturation region where only asymmetric hydrogen-bonded dimers are observed corresponds to conditions known to lead the system toward the nucleation and growth of the β

https://dx.doi.org/10.1021/acs.cgd.0c01257
Cryst. Growth Des. XXXX, XXX, XXX−XXX

form. The high supersaturation conditions where we begin to record statistically significant concentrations of symmetric carboxylic−carboxylic hydrogen-bonded dimers instead correspond to conditions known to lead to the α form, which contains the centrosymmetric dimer as characteristic constitutive building unit.

Ethanol and Acetone Solution. Molecular aggregates in ethanol and acetone showed larger diversity in size than in water solutions; nevertheless, the dominant self-associated species remained the dimer. The overall fraction of self-associated pABA molecules in acetone was found in a range from ∼40% in undersaturated system *ss0.8* up to ∼80% in supersaturated system *ss1.5*. The fraction of self-associated pABA molecules were even higher in ethanol solution and varied from ∼50% to nearly 100%, respectively. It is worth noting that pABA solubility in organic solvents is more than 20 times higher than that in water. Therefore, the considerably larger fraction of self-associated molecules observed is likely due to the higher density of pABA molecules found in ethanol and acetone compared to water in similar saturation conditions. Nevertheless, the spontaneous formation of large, dense pABA aggregates that might be considered as crystal nuclei were not observed in ethanol and acetone even in supersaturated system *ss1.5*, indicating that the nucleation time scale extends well beyond the time scale of the simulations performed in this study.

The free energy surface as a function of distance and angle between self-associated pABA molecules exhibits two basins (Figure 6). The most populated one is at pABA intermolecular distance ∼10 Å and the intermolecular angle between $\pi/2$ and π. This basin corresponds to pABA hydrogen-bonded dimers, where molecules with a relative intermolecular angle close to $\pi/2$ form a carboxylic−amino hydrogen bond. Whereas at values of the intermolecular angle equal to π-carboxylic−carboxylic or amino−amino hydrogen bonds are represented. The second basin covers intermolecular distances between 7 and 8 Å, has a lower angular preference, and corresponds to mostly *T-shaped* $\pi-\pi$ stacked aggregates.

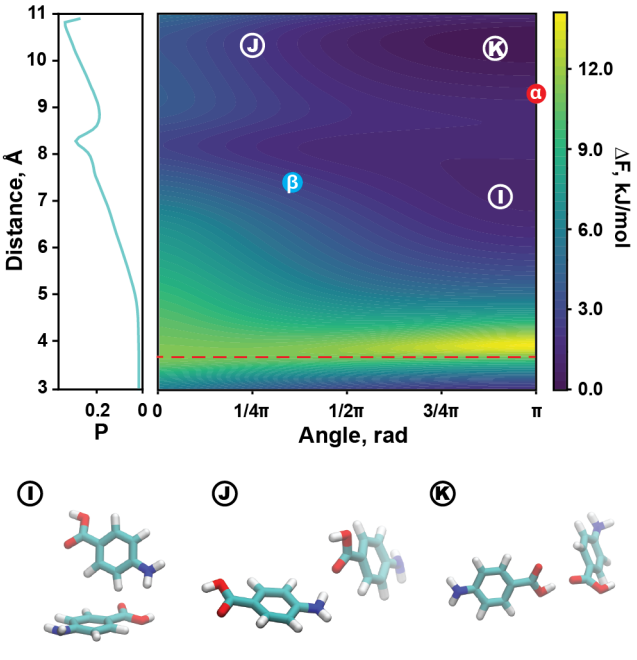

Figure 6. Top: Free energy profile of self-associated pABA dimers in acetone solution *ss1.1* as a function of intermolecular pABA distance and relative orientation. Red dashed line represents intermolecular distance in *face-to-face* $\pi-\pi$ stacked dimers. Red circle indicates location of α form dimer on the FES; blue indicates the β form. Bottom: representative pABA dimers from MD simulations with their location indicated on the FES.

Aromatic Interactions. The fraction of $\pi-\pi$ stacked pABA molecules in acetone was similar to that in water, whereas in ethanol $\pi-\pi$ stacked pABA aggregates were about twice as common (Table 1). There were no noticeable differences in stacked pABA aggregate arrangement from solvent to solvent, and molecule relative orientation in stacked pABA aggregates was the same as in water. The ratio of various stacking types, however, changed significantly. In both organic solvents *T-shaped* stacking was preferred, with 65% of pABA molecules involved in this kind of interaction in acetone and ∼50% in ethanol. The fraction of *T-shaped* aggregates increased mostly at the expense of *offset* $\pi-\pi$ stacked dimers. These substantial differences in the stacked aggregate ratio are the reason $\pi-\pi$ aggregate basin in the distance-angle FES (Figure 6) had noticeably different shape than in water, and average distance in $\pi-\pi$ stacked aggregates was slightly larger.

The average lifetime of the $\pi-\pi$ stacked aggregates in organic solvents was slightly shorter than that in water: ∼50 ps in ethanol and ∼33 ps in acetone.

Hydrogen Bonding. As mentioned earlier, the probability of encountering hydrogen-bonded pABA aggregates in organic solvents is several orders of magnitude higher than that in water (Table 1). Just like with $\pi-\pi$ stacking, hydrogen bonding increases noticeably with an increase in solution concentration. The fraction of pABA molecules involved in hydrogen bonding ranged from 35% in undersaturated acetone *ss0.8*, up to 68% in supersaturated acetone *ss1.5*. In ethanol, the fraction of hydrogen-bonded molecules ranged from 46.1% to 86.4%, moving from undersaturated to supersaturated solutions. The fact that, compared to water, hydrogen bonding in acetone and ethanol is considerably more favorable is consistent with the assumption that hydrogen bonding affects self-association by solvating the carboxylic and amino groups, thus disrupting pABA hydrogen-bonded self-associates.

The preferred hydrogen-bonded pABA aggregate in acetone solution was the carboxylic−carboxylic dimer, accounting for ∼50% of all hydrogen-bonded aggregates. In ethanol instead, carboxylic−amino and carboxylic−carboxylic hydrogen bonding were equally favored (∼45% each). The fraction of amino−amino hydrogen bonding did not display a marked change, moving from ∼5% in acetone to ∼10% in ethanol. The relative importance of different hydrogen-bonded aggregate types did not display a marked dependence on solution concentration. The expected pABA building block—i.e. the symmetric carboxylic−carboxylic hydrogen-bonded pABA dimer—was observed in organic solvent solutions, accounting for ∼20% of all carboxylic−carboxylic pABA dimers in acetone and ∼13% in ethanol.

This observation is coherent with the assumption that solvents able to hydrogen bond the pABA polar moieties inhibit the formation of pABA H-bonded dimers. We find that this effect impacts significantly the relative abundance of symmetric H-bonded dimers, which in order to be assembled in solution require the simultaneous desolvation of the carboxylic groups of two nearby pABA molecules. Therefore,

https://dx.doi.org/10.1021/acs.cgd.0c01257
Cryst. Growth Des. XXXX, XXX, XXX−XXX

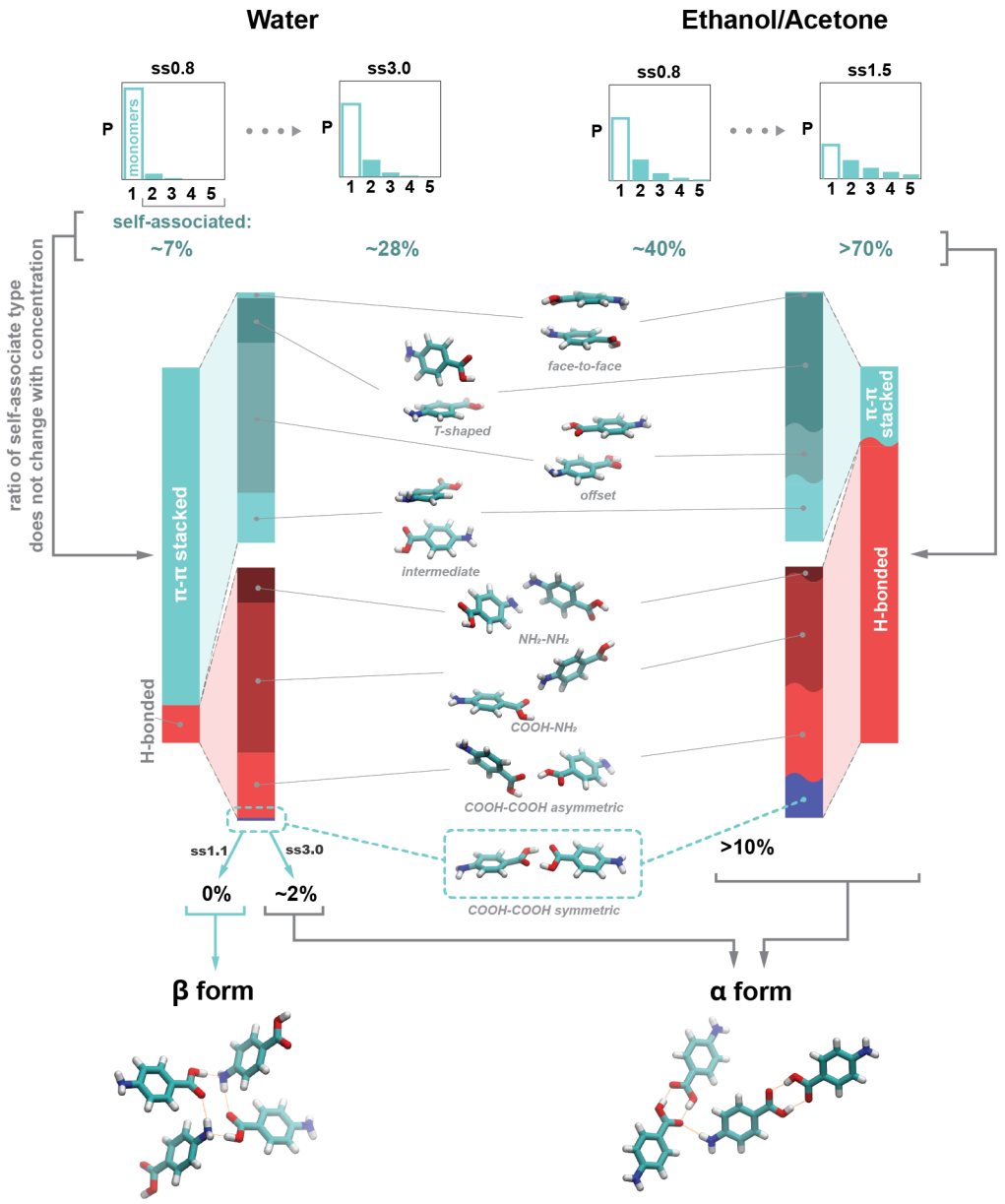

Figure 7. Schematic summary of pABA molecule distribution in various self-associate species depending on the solvent used. The top part of the figure shows the probability of pABA molecule to be part of self-associated aggregates of a specific size at various concentrations and solvents. The dominant pABA species in all systems studied is a monomer, whereas the most abundant pABA aggregate is a dimer. The central panel of the figure reports the ratio of various self-associate types in the solvents studied. The outer stacked bar graph displays the relative probability of pABA molecules involved in $\pi-\pi$ stacked (cyan) and hydrogen-bonded (red) self-associates. The inner bar graph provides a further breakdown of each $\pi-\pi$ stacked and hydrogen-bonded dimer motif. The average probability of acetone and ethanol systems are shown. Illustration of each self-associate motif is given in the central section of the figure. The fraction of symmetric carboxylic dimers in water (blue in bar graphs) was found to be dependent on concentration. Carboxylic−carboxylic dimers were exclusively asymmetric at low concentrations (*ss1.1*), known to yield the β form. At higher concentrations instead (*ss3.0*), where the α form is produced, symmetric carboxylic−carboxylic dimers were observed with a low, but statistically significant, probability.

the formation of symmetric H-bonded dimers in hydrogen-bonding solvent is very unlikely, while in aprotic solvents the probability of observing this type of self-association is significantly higher. The fraction of symmetric pABA dimers did no change with solution concentration. Finally the lifetime of hydrogen-bonded dimers was considerably longer in organic solvents with respect to water, and it did not display a marked dependence on solution concentration.

The lifetime of hydrogen-bonded dimers was considerably longer in organic solvents and did not change with solution concentration. On average, pABA intermolecular hydrogen bonds in water lasted for ~28 ps, whereas in ethanol and acetone, the lifetimes of hydrogen bonded dimers were ~85 ps and ~93 ps, respectively.

Aggregates Lifetime. An analysis of the aggregates average lifetime across all solvent considered shows that all the complex species identified as statistically relevant in aqueous solution possess a fluxional character, reversibly assembling, disassembling, and changing the internal structure very rapidly. In aqueous solution, the average lifetime of $\pi-\pi$ stacked dimers is shorter than 100 ps, while hydrogen-bonded complexes reach up to 30 ps at the highest concentrations

https://dx.doi.org/10.1021/acs.cgd.0c01257
Cryst. Growth Des. XXXX, XXX, XXX−XXX

considered in this study. In the organic solvents considered in this study, hydrogen-bonded self-associates are longer lived than those stabilized by aromatic stacking. Aggregate lifetimes on the same order of magnitude were also noted for reference compounds (see Supporting Information).

This observation strongly suggests that the dominant growth unit of pABA crystals is not a self-associated pABA complex but rather a monomer. This interpretation of our results supports the view emerging from the work of Cruz-Cabeza et al.[71] that identifies in the stability of monomers aromatic stacking an important factor correlating with nucleation rates across a range of systems and solvents.

DISCUSSION AND CONCLUSIONS

In this work by combining NMR spectroscopy and MD calculations, we demonstrate that pABA self-association is not only solvent-dependent but also remarkably dynamical. NMR experiments provide a clear indication that different intermolecular interactions drive self-association in different solvents. This observation is confirmed in MD simulations, which provide a wealth of details regarding the diversity of the configurational ensemble of pABA self-associates.

MD simulations indicate that while monomers are the most common species in all solutions, self-associates can be found in all solutions studied. For instance, the fraction of self-associated pABA molecules in water ranges from 7% in undersaturated solution (*ss0.8*) up to ∼28% in highly supersaturated solutions (*ss3.0*), whereas in acetone and ethanol nearly half of the pABA molecules are involved in some kind of self-association even in undersaturated solutions (Figure 7). As indicated by both NMR and MD, the dominant pABA self-associates in acetone and ethanol are stabilized by hydrogen-bonding, whereas in water the $\pi-\pi$ stacking dominates. These results support the consolidated view that solvents with low polarity and weak hydrogen-bonding character favor the formation of pABA−pABA hydrogen-bonded dimers. Polar solvents that are good hydrogen bond donors instead can efficiently solvate carboxylic groups, thus limiting the formation of pABA hydrogen-bonded dimers.[64,65,70]

In all cases, self-associates establish a dynamic equilibrium with monomers in solution, characterized by rapid exchanges of monomers that take place on a time scale of the order of 100 ps.

The structural diversity and short lifetime of self-associates suggest that the growth unit determining the assembly of pABA crystals in solution is likely to be a monomer rather than a dimer preassembled, in a specific configuration. This observation is consistent with the fact that the kinetics of nucleation and growth of α pABA crystals are primarily controlled by aromatic stacking.[68,71]

Despite dominant interactions vary between different solutions. In all cases, self-associates populate a diverse ensemble of configurations which includes both $\pi-\pi$ stacking and H-bonding motifs. H-bonded dimers are therefore consistently found also in aqueous solutions, even if at much lower concentrations than in organic solvents, and predominantly involved in asymmetric, single H-bond dimers.

For instance, in highly supersaturated water solutions the equilibrium probability of finding symmetric carboxylic−carboxylic hydrogen-bonded dimers is 1 order of magnitude lower than the probability of observing asymmetric H-bonded dimers, while at low supersaturation (<1.5) the symmetric carboxylic−carboxylic hydrogen-bond motif becomes completely inaccessible. This result is consistent with neutron scattering data[70] of the structurally similar benzoic acid in methanol, which suggested that besides $\pi-\pi$ stacking and weak carboxylic−aromatic proton interactions, benzoic acid molecules exist in mostly asymmetric hydrogen-bonded motifs rather than as symmetric carboxyl−carboxyl hydrogen-bonded complexes.

In light of these observations, we interpret the presence of symmetric H-bonded carboxylic dimers as indicative of the fact that the simultaneous desolvation of two carboxylic groups is statistically accessible. In such conditions pABA crystallization leads to the α form. Conversely, the β form is favored in solutions where strong solvation of carboxylic moieties completely suppresses the formation of symmetric H-bonded motifs.

To conclude, this work reconciles several observations on pABA solutions and shows that including dynamics and finite-temperature effects in the description of the solution structure is key to understand how solution composition affects polymorph selection.

METHODS

NMR Spectroscopy. ^{1}H and ^{13}C NMR spectra of *p*-aminobenzoic acid, cyclohexane carboxylic acid, toluene, (dimethoxymethyl)-benzene and *p*-aminocyclohexane carboxylic acid in deuterium oxide, ethanol-d_6 and acetone-d_6 were recorded at 298 K on a 600 MHz Bruker Avance Neo spectrometer equipped with a QCI quadruple-resonance pulsed-field-gradient cryoprobe. Solute concentrations ranged from 1 mol L^{-1} to 10 μmol L^{-1}. For systems where the desired maximum concentration of 1 mol L^{-1} cannot be achieved due to poor solubility, the range up to saturation concentration was covered. The most concentrated solution in each solvent was prepared directly, while the rest of the solutions were prepared by subsequent dilution. An analytical balance (±0.1 mg) and micropipettes (±0.1 μL) were used for solution preparation. NMR spectra of solutions were recorded right after solution preparation. Acetone-d_6 or methanol-d_4 was used as an external reference (in 3 mm NMR tube that was inserted in the sample tube) for chemical shift displacement calculation. The spectra were processed using Bruker Topspin 4.0.8.

NMR Experimental Parameters. ^{13}C NMR spectra were acquired using the following parameters: pulse width 3.67 μs (30°), 236.72 ppm spectral width, 0.92 s acquisition time, 32−16384 scans depending on the compound concentration, 2 s recycle delay, and 65536 acquired total data points.

MD Calculations. *Forcefield.* Forcefields for *p*-aminobenzoic acid; NMR reference compounds, cyclohexane carboxylic acid, toluene, (dimethoxymethyl)benzene, and *p*-aminocyclohexane carboxylic acid; and solvents used, ethanol and acetone, were based on the general AMBER force field (GAFF) and were generated using ambertools.[83−85] The quality of the derived forcefield parameters were evaluated by comparing the calculated densities and enthalpy of vaporisation to experimentally determined values. Water was described by the TIP3P model.

MD Simulation. Unbiased MD simulations were performed for pABA and the NMR reference compounds in water, ethanol, and acetone at various concentrations. pABA systems were prepared at solution concentrations that correspond to supersaturations 0.8, 1.1, and 1.5. For the pABA water system, additional simulations were performed at supersaturations 2.0 and 3.0. Systems with desired solute concentrations were prepared by inserting an appropriate amount of solute molecules in a 10 × 10 × 10 nm box and then by filling the box with the respective solvent. NMR reference compound systems were prepared at a concentration that corresponds to the higher concentrations used in NMR experiments—1 mol L^{-1}, unless solubility was lower—then saturated solution was prepared. Since solubility for several reference systems was poor, and in some cases, it

https://dx.doi.org/10.1021/acs.cgd.0c01257
Cryst. Growth Des. XXXX, XXX, XXX−XXX

would require only one solute molecule in a simulation box of comparable size to those used to study pABA water system, was used. In these cases, 30 solute molecules were placed in 10 × 10 × 10 nm simulation box.

The prepared systems were relaxed through an energy minimization, performed using the steepest descent algorithm with a tolerance of 100 kJ mol^{-1} nm^{-1}. After minimization, all systems were equilibrated in the *NVT* and then *NPT* ensembles for 5 ns. The MD (leapfrog) integration scheme with an integration time step of 2 fs was employed for equilibration and production runs. The particle mesh Ewald (PME) approach was used to calculate long-range electrostatic interactions, with a cutoff of 0.8 nm. Both Lennard-Jones and Coulomb interactions were explicitly calculated up to 0.8 nm. The LINCS algorithm[86] was applied at each step to preserve the hydrogen bond lengths. *NPT* equilibration was performed employing a Berendsen barostat[87] with a coupling constant of 2 ps and reference pressure 1.0 bar. Velocity-rescale thermostat[88] with a coupling constant of 2 ps and reference temperature 298.0 K was used for equilibration and production simulations. The production runs were performed in the *NPT* ensemble for 100 ns. System coordinates were saved every 10 ps and a total of 10000 frames were generated for further analysis. The potential energy minimization and MD simulations were carried out with the software package Gromacs 2018.2,[89,90] applying periodic boundary conditions.

Trajectory Analysis. Trajectory analysis was performed using Plumed 2.5[59,91] and in-house python scripts. Solute molecule $\pi-\pi$ stacking was identified by checking the distance between benzene ring centers, and angles between adjacent molecules (Figure 8 left).

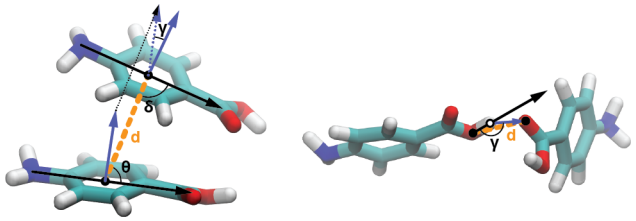

Figure 8. Graphical representation of vectors, distances and angles used in self-associate recognition and characterization. Left: in the case of $\pi-\pi$ stacking (black, molecule vector; blue, normal to the benzene ring plane; orange dashed line, distance between molecule centers). Right: in the case of hydrogen bonding (black, vector from hydrogen bond donor heteroatom to proton; blue, vector from proton to hydrogen bond accepting heteroatom; orange dashed line, distance between two hetero atoms involved in hydrogen bonding).

Hydrogen bonding was identified by checking the distance between proton donor and acceptor atoms, and by computing the angle between the vector that is defined from the hydrogen bond donor to the proton and the vector defined between the proton and the hydrogen bond acceptor (Figure 8 right). Parameters[82,92] used for self-associate recognition are summarized in Table 2. Symmetric carboxylic−carboxylic hydrogen-bonded dimers were identified by checking whether both carboxylic group oxygen atoms are involved in hydrogen bonding with each other. The free energy profiles $F(S)$ were calculated as $F(S) = -k_BT \ln p(S)$, where k_B is the Boltzmann's constant, T is the temperature, and $p(S)$ is the probability density function of S, a descriptor of the state of the system.

■ ASSOCIATED CONTENT

Supporting Information

The Supporting Information is available free of charge at https://pubs.acs.org/doi/10.1021/acs.cgd.0c01257.

MD simulation results of reference compounds, analysis of pABA conformational isomerism in solution, and additional details on estimates of aggregates lifetime (PDF)

■ AUTHOR INFORMATION

Corresponding Authors

Raitis Bobrovs − *Latvian Institute of Organic Synthesis, LV-1006 Riga, Latvia*; Email: raitis.bobrovs@osi.lv

Matteo Salvalaglio − *Thomas Young Centre and Department of Chemical Engineering, University College London, London WC1E 7JE, U.K.*; orcid.org/0000-0003-3371-2090; Email: m.salvalaglio@ucl.ac.uk

Authors

Laura Drunka − *Latvian Institute of Organic Synthesis, LV-1006 Riga, Latvia*

Andrievs Auseklis Auzins − *Latvian Institute of Organic Synthesis, LV-1006 Riga, Latvia*

Kristaps Jaudzems − *Latvian Institute of Organic Synthesis, LV-1006 Riga, Latvia*; orcid.org/0000-0003-3922-2447

Complete contact information is available at: https://pubs.acs.org/10.1021/acs.cgd.0c01257

Notes

The authors declare no competing financial interest.

■ ACKNOWLEDGMENTS

This research is funded by the Latvian Council of Science, for the project "From molecules to crystals: molecular self-assembly in crystal nucleation from solution", Project No. lzp-2018/2-0234. Professor Sally Price is acknowledged for fruitful discussions and feedback on an early version of the manuscript. Calculations were performed on University College London's Legion, Myriad, and Grace High Performance Computing Facilities.

Table 2. Distance and Angle Values Used in Self-associate Recognition and Characterization[a]

	d, Å	γ, rad	θ, rad	δ, rad
		$\pi-\pi$ stacking		
none	>6.0	−	<π/6 (30°)	<π/6 (30°)
T-shaped	≤5.6	>5π/18 (50°)	−	−
face-to-face	≤5.6	<π/6 (30°)	>4π/9 (80°)	−
offset	≤5.6	<π/6 (30°)	<4π/9 (80°)	−
intermediate	≤5.6	>π/6 (30°)	−	−
		hydrogen bonding		
hydrogen bond	≤3.2	>18π/25 (130°)		

[a]Depiction of parameters is available in Figure 8.

https://dx.doi.org/10.1021/acs.cgd.0c01257
Cryst. Growth Des. XXXX, XXX, XXX−XXX

REFERENCES

(1) Mullin, J. W. *Crystallization*, 4th ed.; Butterworth-Heinemann: Oxford, 2001; p 600.
(2) Erdemir, D.; Lee, A. Y.; Myerson, A. S. Nucleation of crystals from solution: classical and two-step models. *Acc. Chem. Res.* **2009**, *42*, 621−629.
(3) Myerson, a. S.; Trout, B. L. Nucleation from Solution. *Science* **2013**, *341*, 855−856.
(4) Hamad, S.; Moon, C.; Catlow, C. R. A.; Hulme, A. T.; Price, S. L. Kinetic Insights into the Role of the Solvent in the Polymorphism of 5-Fluorouracil from Molecular Dynamics Simulations. *J. Phys. Chem. B* **2006**, *110*, 3323−3329.
(5) Tung, H.-H.; Paul, E. L.; Midler, M.; McCauley, J. A. *Crystallization of Organic Compounds: An Industrial Perspective*; John Wiley & Sons, Inc.: Hoboken, NJ, 2009; p 304.
(6) Chattopadhyay, S.; Erdemir, D.; Evans, J. M. B.; Ilavsky, J.; Amenitsch, H.; Segre, C. U.; Myerson, A. S. SAXS Study of the Nucleation of Glycine Crystals from a Supersaturated Solution. *Cryst. Growth Des.* **2005**, *5*, 523−527.
(7) Chen, C.; Cook, O.; Nicholson, C. E.; Cooper, S. J. Leapfrogging Ostwald's rule of stages: Crystallization of stable γ-glycine directly from microemulsions. *Cryst. Growth Des.* **2011**, *11*, 2228−2237.
(8) Chen, X.; Schröder, J.; Hauschild, S.; Rosenfeldt, S.; Dulle, M.; Förster, S. Simultaneous SAXS/WAXS/UV-Vis Study of the Nucleation and Growth of Nanoparticles: A Test of Classical Nucleation Theory. *Langmuir* **2015**, *31*, 11678−11691.
(9) Pontoni, D.; Narayanan, T.; Rennie, A. R. Time-resolved SAXS study of nucleation and growth of silica colloids. *Langmuir* **2002**, *18*, 56−59.
(10) Toroz, D.; Rosbottom, I.; Turner, T. D.; Corzo, D. M.; Hammond, R. B.; Lai, X.; Roberts, K. J. Towards an understanding of the nucleation of alpha-para amino benzoic acid from ethanolic solutions: A multi-scale approach. *Faraday Discuss.* **2015**, *179*, 79−114.
(11) Regev, O. Nucleation events during the synthesis of mesoporous materials using liquid crystalline templating. *Langmuir* **1996**, *12*, 4940−4944.
(12) Pouget, E. M.; Bomans, P. H. H.; Goos, J. A. C. M.; Frederik, P. M.; de With, G.; Sommerdijk, N. A. J. M. The Initial Stages of Template-Controlled CaCO3 Formation Revealed by Cryo-TEM. *Science* **2009**, *323*, 1455−1458.
(13) Bonini, M.; Rossi, S.; Karlsson, G.; Almgren, M.; Lo Nostro, P.; Baglioni, P. Self-Assembly of β-Cyclodextrin in Water. Part 1: Cryo-TEM and Dynamic and Static Light Scattering. *Langmuir* **2006**, *22*, 1478−1484.
(14) Rieger, J.; Frechen, T.; Cox, G.; Heckmann, W.; Schmidt, C.; Thieme, J. Precursor structures in the crystallization/precipitation processes of CaCO3 and control of particle formation by polyelectrolytes. *Faraday Discuss.* **2007**, *136*, 265−277.
(15) Lee, J.; Saha, A.; Pancera, S. M.; Kempter, A.; Rieger, J.; Bose, A.; Tripathi, A. Shear free and blotless cryo-TEM imaging: A new method for probing early evolution of nanostructures. *Langmuir* **2012**, *28*, 4043−4046.
(16) Baumgartner, J.; Dey, A.; Bomans, P. H.; Le Coadou, C.; Fratzl, P.; Sommerdijk, N. A.; Faivre, D. Nucleation and growth of magnetite from solution. *Nat. Mater.* **2013**, *12*, 310−314.
(17) Kellermeier, M.; Gebauer, D.; Melero-García, E.; Drechsler, M.; Talmon, Y.; Kienle, L.; Cölfen, H.; García-Ruiz, J. M.; Kunz, W. Colloidal stabilization of calcium carbonate prenucleation clusters with silica. *Adv. Funct. Mater.* **2012**, *22*, 4301−4311.
(18) Nielsen, M. H.; Aloni, S.; De Yoreo, J. J. In situ TEM imaging of CaCO3 nucleation reveals coexistence of direct and indirect pathways. *Science* **2014**, *345*, 1158−1162.
(19) De Yoreo, J. Crystal nucleation: more than one pathway. *Nat. Mater.* **2013**, *12*, 284−5.
(20) Tsarfati, Y.; Rosenne, S.; Weissman, H.; Shimon, L. J.; Gur, D.; Palmer, B. A.; Rybtchinski, B. Crystallization of Organic Molecules: Nonclassical Mechanism Revealed by Direct Imaging. *ACS Cent. Sci.* **2018**, *4*, 1031−1036.
(21) Zhou, J.; Yang, Y.; Yang, Y.; Kim, D. S.; Yuan, A.; Tian, X.; Ophus, C.; Sun, F.; Schmid, A. K.; Nathanson, M.; Heinz, H.; An, Q.; Zeng, H.; Ercius, P.; Miao, J. Observing crystal nucleation in four dimensions using atomic electron tomography. *Nature* **2019**, *570*, 500−503.
(22) Huggins, C. M.; Pimentel, G. C.; Shoolery, J. N. Proton Magnetic Resonance Studies of the Hydrogen Bonding of Phenol, Substituted Phenols and Acetic Acid. *J. Phys. Chem.* **1956**, *60*, 1311−1315.
(23) Becker, E. D.; Liddel, U.; Shoolery, J. N. Nuclear magnetic resonance studies of hydrogen bonding in ethanol. *J. Mol. Spectrosc.* **1958**, *2*, 1−8.
(24) Pastor, A.; Martínez-Viviente, E. NMR spectroscopy in coordination supramolecular chemistry: A unique and powerful methodology. *Coord. Chem. Rev.* **2008**, *252*, 2314−2345.
(25) Vioglio, P. C.; Thureau, P.; Juramy, M.; Ziarelli, F.; Viel, S.; Williams, P. A.; Hughes, C. E.; Harris, K. D.; Mollica, G. A Strategy for Probing the Evolution of Crystallization Processes by Low-Temperature Solid-State NMR and Dynamic Nuclear Polarization. *J. Phys. Chem. Lett.* **2019**, *10*, 1505−1510.
(26) Cerreia Vioglio, P.; Mollica, G.; Juramy, M.; Hughes, C. E.; Williams, P. A.; Ziarelli, F.; Viel, S.; Thureau, P.; Harris, K. D. Insights into the Crystallization and Structural Evolution of Glycine Dihydrate by In Situ Solid-State NMR Spectroscopy. *Angew. Chem., Int. Ed.* **2018**, *57*, 6619−6623.
(27) Hughes, C. E.; Williams, P. A.; Kariuki, B. M.; Harris, K. D. Establishing the Transitory Existence of Amorphous Phases in Crystallization Pathways by the CLASSIC NMR Technique. *ChemPhysChem* **2018**, *19*, 3341−3345.
(28) Schulze, B. M.; Watkins, D. L.; Zhang, J.; Ghiviriga, I.; Castellano, R. K. Estimating the shape and size of supramolecular assemblies by variable temperature diffusion ordered spectroscopy. *Org. Biomol. Chem.* **2014**, *12*, 7932−7936.
(29) Ferrazza, R.; Rossi, B.; Guella, G. DOSY-NMR and raman investigations on the self-aggregation and cyclodextrin complexation of vanillin. *J. Phys. Chem. B* **2014**, *118*, 7147−7155.
(30) Hughes, C. E.; Williams, P. A.; Harris, K. D. M. An In-Situ NMR Strategy for Mapping the Time- Evolution of Crystallization Processes by Combined Liquid-State and Solid-State Measurements. *Angew. Chem., Int. Ed.* **2014**, *53*, 8939−8943.
(31) Hunter, C. A.; McCabe, J. F.; Spitaleri, A. Solvent effects of the structures of prenucleation aggregates of carbamazepine. *CrystEngComm* **2012**, *14*, 7115−7117.
(32) Spitaleri, A.; Hunter, C. A.; McCabe, J. F.; Packer, M. J.; Cockroft, S. L. A 1H NMR study of crystal nucleation in solution. *CrystEngComm* **2004**, *6*, 489−493.
(33) Hunter, C. A.; Packer, M. J. Complexation-Induced Changes in1H NMR Chemical Shift for Supramolecular Structure Determination. *Chem. - Eur. J.* **1999**, *5*, 1891−1897.
(34) Musumeci, D.; Hunter, C. A.; McCabe, J. F. Solvent Effects on Acridine Polymorphism. *Cryst. Growth Des.* **2010**, *10*, 1661−1664.
(35) Gmeiner, W. H.; Poulter, C. D. NMR studies of nucleic acids. Deuterium isotope effects on carbon-13 chemical shifts in hydrogen-bonded complexes of pyrimidines and purines. *J. Am. Chem. Soc.* **1988**, *110*, 7640−7647.
(36) Bobrovs, R.; Seton, L.; Dempster, N. The reluctant polymorph: investigation into the effect of self-association on the solvent mediated phase transformation and nucleation of theophylline. *CrystEngComm* **2015**, *17*, 5237−5251.
(37) Peral, F.; Gallego, E. Self-association of pyrimidine and some of its methyl derivatives in aqueous solution. *J. Mol. Struct.* **1995**, *372*, 101−112.
(38) Dearden, J. C. Investigation of the Self-Association of Phenols and Anilines By Ultraviolet Spectroscopy. *Can. J. Chem.* **1963**, *41*, 2683−2691.
(39) Singh, S.; Rao, C. N. R. Spectroscopic studies of self-association due to hydrogen bonding. *J. Phys. Chem.* **1967**, *71*, 1074−1078.
(40) Davey, R. J.; Dent, G.; Mughal, R. K.; Parveen, S. Concerning the Relationship between Structural and Growth Synthons in Crystal

https://dx.doi.org/10.1021/acs.cgd.0c01257
Cryst. Growth Des. XXXX, XXX, XXX−XXX

Nucleation: Solution and Crystal Chemistry of Carboxylic Acids As Revealed through IR Spectroscopy. *Cryst. Growth Des.* **2006**, *6*, 1788−1796.
(41) Kulkarni, S. A.; McGarrity, E. S.; Meekes, H.; ter Horst, J. H. Isonicotinamide self-association: the link between solvent and polymorph nucleation. *Chem. Commun.* **2012**, *48*, 4983−5.
(42) Sullivan, R. A.; Davey, R. J.; Sadiq, G.; Dent, G.; Back, K. R.; Ter Horst, J. H.; Toroz, D.; Hammond, R. B. Revealing the roles of desolvation and molecular self-assembly in crystal nucleation from solution: Benzoic and p -aminobenzoic acids. *Cryst. Growth Des.* **2014**, *14*, 2689−2696.
(43) Tang, W.; Zhang, M.; Mo, H.; Gong, J.; Wang, J.; Li, T. Higher-order self-assembly of benzoic acid in solution. *Cryst. Growth Des.* **2017**, *17*, 5049−5053.
(44) Sosso, G. C.; Chen, J.; Cox, S. J.; Fitzner, M.; Pedevilla, P.; Zen, A.; Michaelides, A. Crystal Nucleation in Liquids: Open Questions and Future Challenges in Molecular Dynamics Simulations. *Chem. Rev.* **2016**, *116*, 7078−7116.
(45) Matsumoto, M.; Saito, S.; Ohmine, I. Molecular dynamics simulation of the ice nucleation and growth process leading to water freezing. *Nature* **2002**, *416*, 409−13.
(46) Gavezzotti, a. Molecular Aggregation of Acetic Acid in a Carbon Tetrachloride Solution: A Molecular Dynamics Study with a View to Crystal Nucleation. *Chem. - Eur. J.* **1999**, *5*, 567−576.
(47) Tribello, G. a.; Bruneval, F.; Liew, C.; Parrinello, M. A molecular dynamics study of the early stages of calcium carbonate growth. *J. Phys. Chem. B* **2009**, *113*, 11680−11687.
(48) Shah, M.; Santiso, E. E.; Trout, B. L. Computer simulations of homogeneous nucleation of benzene from the melt. *J. Phys. Chem. B* **2011**, *115*, 10400−10412.
(49) Santiso, E. E.; Trout, B. L. A general set of order parameters for molecular crystals. *J. Chem. Phys.* **2011**, *134*, 064109.
(50) Salvalaglio, M.; Vetter, T.; Giberti, F.; Mazzotti, M.; Parrinello, M. Uncovering Molecular Details of Urea Crystal Growth in the Presence of Additives. *J. Am. Chem. Soc.* **2012**, *134*, 17221−17233.
(51) Salvalaglio, M.; Vetter, T.; Mazzotti, M.; Parrinello, M. Controlling and predicting crystal shapes: The case of urea. *Angew. Chem.* **2013**, *125*, 13611−13614.
(52) Wallace, A. F.; Hedges, L. O.; Fernandez-Martinez, A.; Raiteri, P.; Gale, J. D.; Waychunas, G. a.; Whitelam, S.; Banfield, J. F.; De Yoreo, J. J. Microscopic evidence for liquid-liquid separation in supersaturated CaCO3 solutions. *Science* **2013**, *341*, 885−889.
(53) Di Tommaso, D. The molecular self-association of carboxylic acids in solution: testing the validity of the link hypothesis using a quantum mechanical continuum solvation approach. *CrystEngComm* **2013**, *15*, 6564.
(54) Salvalaglio, M.; Giberti, F.; Parrinello, M. 1,3,5-Tris(4-bromophenyl)benzene prenucleation clusters from meta-dynamics. *Acta Crystallogr., Sect. C: Struct. Chem.* **2014**, *70*, 132−136.
(55) Salvalaglio, M.; Perego, C.; Giberti, F.; Mazzotti, M.; Parrinello, M. Molecular-dynamics simulations of urea nucleation from aqueous solution. *Proc. Natl. Acad. Sci. U. S. A.* **2015**, *112*, E6−E14.
(56) Giberti, F.; Salvalaglio, M.; Parrinello, M. Metadynamics studies of crystal nucleation. *IUCrJ* **2015**, *2*, 256−266.
(57) Giberti, F.; Salvalaglio, M.; Mazzotti, M.; Parrinello, M. Insight into the nucleation of urea crystals from the melt. *Chem. Eng. Sci.* **2015**, *121*, 51−59.
(58) Giberti, F.; Salvalaglio, M.; Mazzotti, M.; Parrinello, M. 1,3,5-tris(4-bromophenyl)-benzene Nucleation: From Dimers to Needle-like Clusters. *Cryst. Growth Des.* **2017**, *17*, 4137−4143.
(59) Tribello, G. A.; Giberti, F.; Sosso, G. C.; Salvalaglio, M.; Parrinello, M. Analyzing and Driving Cluster Formation in Atomistic Simulations. *J. Chem. Theory Comput.* **2017**, *13*, 1317−1327.
(60) Rosbottom, I.; Yong, C. W.; Geatches, D. L.; Hammond, R. B.; Todorov, I. T.; Roberts, K. J. The integrated DL_POLY/DL_FIELD/DL_ANALYSER software platform for molecular dynamics simulations for exploration of the synthonic interactions in saturated benzoic acid/hexane solutions. *Mol. Simul.* **2019**, *0*, 1−16.
(61) Gobbo, G.; Bellucci, M. A.; Tribello, G. A.; Ciccotti, G.; Trout, B. L. Nucleation of Molecular Crystals Driven by Relative Information Entropy. *J. Chem. Theory Comput.* **2018**, *14*, 959−972.
(62) Benali-Cherif, R.; Takouachet, R.; Bendeif, E. E.; Benali-Cherif, N. The structural properties of a noncentrosymmetric polymorph of 4-aminobenzoic acid. *Acta Crystallogr., Sect. C: Struct. Chem.* **2014**, *70*, 323−325.
(63) Ward, M. R.; Younis, S.; Cruz-Cabeza, A. J.; Bull, C. L.; Funnell, N. P.; Oswald, I. D. Discovery and recovery of delta p-aminobenzoic acid. *CrystEngComm* **2019**, *21*, 2058−2066.
(64) Gracin, S.; Rasmuson, Å. C. Polymorphism and Crystallization of p -Aminobenzoic Acid. *Cryst. Growth Des.* **2004**, *4*, 1013−1023.
(65) Svärd, M.; Nordström, F. L.; Hoffmann, E. M.; Aziz, B.; Rasmuson, Å. C. Thermodynamics and nucleation of the enantiotropic compound p-aminobenzoic acid. *CrystEngComm* **2013**, *15*, 5020−5031.
(66) Hao, H.; Barrett, M.; Hu, Y.; Su, W.; Ferguson, S.; Wood, B.; Glennon, B. The use of in situ tools to monitor the enantiotropic transformation of p-aminobenzoic acid polymorphs. *Org. Process Res. Dev.* **2012**, *16*, 35−41.
(67) Black, J. F.; Davey, R. J.; Gowers, R. J.; Yeoh, A. Ostwald's rule and enantiotropy: Polymorph appearance in the crystallisation of p-aminobenzoic acid. *CrystEngComm* **2015**, *17*, 5139−5142.
(68) Black, J. F.; Cardew, P. T.; Cruz-Cabeza, A. J.; Davey, R. J.; Gilks, S. E.; Sullivan, R. A. Crystal nucleation and growth in a polymorphic system: Ostwald's rule,: P -aminobenzoic acid and nucleation transition states. *CrystEngComm* **2018**, *20*, 768−776.
(69) Cruz-Cabeza, A. J.; Davey, R. J.; Oswald, I. D.; Ward, M. R.; Sugden, I. J. Polymorphism in p-aminobenzoic acid. *CrystEngComm* **2019**, *21*, 2034−2042.
(70) Burton, R. C.; Ferrari, E. S.; Davey, R. J.; Finney, J. L.; Bowron, D. T. The relationship between solution structure and crystal nucleation: A neutron scattering study of supersaturated methanolic solutions of benzoic acid. *J. Phys. Chem. B* **2010**, *114*, 8807−8816.
(71) Cruz-Cabeza, A. J.; Davey, R. J.; Sachithananthan, S. S.; Smith, R.; Tang, S. K.; Vetter, T.; Xiao, Y. Aromatic stacking-a key step in nucleation. *Chem. Commun.* **2017**, *53*, 7905−7908.
(72) Cruz-Cabeza, A. J.; Taylor, E.; Sugden, I. J.; Bowskill, D. H.; Wright, S. E.; Abdullahi, H.; Tulegenov, D.; Sadiq, G.; Davey, R. J. Can solvated intermediates inform us about nucleation pathways? The case of *β*-pABA. *CrystEngComm* **2020**, *22*, 7447−7459.
(73) Mattei, A.; Mei, X.; Miller, A.-F.; Li, T. Two Major Pre-Nucleation Species that are Conformationally Distinct and in Equilibrium of Self-Association. *Cryst. Growth Des.* **2013**, *13*, 3303−3307.
(74) Yan, T.; Wang, K.; Duan, D.; Tan, X.; Liu, B.; Zou, B. P-Aminobenzoic acid polymorphs under high pressures. *RSC Adv.* **2014**, *4*, 15534−15541.
(75) Rosbottom, I.; Roberts, K. J.; Docherty, R. The solid state, surface and morphological properties of p-aminobenzoic acid in terms of the strength and directionality of its intermolecular synthons. *CrystEngComm* **2015**, *17*, 5768−5788.
(76) Stevens, J. S.; Gainar, A.; Jaye, C.; Fischer, D. A.; Schroeder, S. L. NEXAFS and XPS of p-Aminobenzoic Acid Polymorphs: The Influence of Local Environment. *J. Phys.: Conf. Ser.* **2016**, *712*, 012133.
(77) Black, J. F.; Cruz-Cabeza, A. J.; Davey, R. J.; Willacy, R. D.; Yeoh, A. The Kinetic Story of Tailor-made Additives in Polymorphic Systems: New Data and Molecular Insights for p-Aminobenzoic Acid. *Cryst. Growth Des.* **2018**, *18*, 7518−7525.
(78) Rosbottom, I.; Toroz, D.; Hammond, R. B.; Roberts, K. J. Conformational and structural stability of the single molecule and hydrogen bonded clusters of para aminobenzoic acid in the gas and solution phases. *CrystEngComm* **2018**, *20*, 7543−7555.
(79) Rosbottom, I.; Pickering, J. H.; Hammond, R. B.; Roberts, K. J. A Digital Workflow Supporting the Selection of Solvents for Optimizing the Crystallizability of p -Aminobenzoic Acid. *Org. Process Res. Dev.* **2020**, *24*, 500−507.

https://dx.doi.org/10.1021/acs.cgd.0c01257
Cryst. Growth Des. XXXX, XXX, XXX−XXX

(80) Turner, T. D.; Corzo, D. M.; Toroz, D.; Curtis, A.; Dos Santos, M. M.; Hammond, R. B.; Lai, X.; Roberts, K. J. The influence of solution environment on the nucleation kinetics and crystallisability of para-aminobenzoic acid. *Phys. Chem. Chem. Phys.* **2016**, *18*, 27507−27520.
(81) Meyer, E. A.; Castellano, R. K.; Diederich, F. Interactions with Aromatic Rings in Chemical and Biological Recognition. *Angew. Chem., Int. Ed.* **2003**, *42*, 1210−1250.
(82) Zhao, Y.; Li, J.; Gu, H.; Wei, D.; Xu, Y.; Fu, W.; Yu, Z. Conformational Preferences of $\pi-\pi$ Stacking Between Ligand and Protein, Analysis Derived from Crystal Structure Data Geometric Preference of $\pi-\pi$ Interaction. *Interdiscip. Sci.: Comput. Life Sci.* **2015**, *7*, 211−220.
(83) Cornell, W. D.; Cieplak, P.; Bayly, C. I.; Gould, I. R.; Merz, K. M.; Ferguson, D. M.; Spellmeyer, D. C.; Fox, T.; Caldwell, J. W.; Kollman, P. A. A Second Generation Force Field for the Simulation of Proteins, Nucleic Acids, and Organic Molecules. *J. Am. Chem. Soc.* **1995**, *117*, 5179−5197.
(84) Wang, J.; Wolf, R. M.; Caldwell, J. W.; Kollman, P. A.; Case, D. A. Development and testing of a general amber force field. *J. Comput. Chem.* **2004**, *25*, 1157−1174.
(85) Case, D.; Ben-Shalom, I.; Brozell, S.; Cerutti, D.; Cheatham, T., III; Cruzeiro, V.; Darden, T.; Duke, R.; Ghoreishi, D.; Gilson, M. et al. *AMBER 2018*. University of California: San Francisco, CA; 2018.
(86) Hess, B. P. P-LINCS: A parallel linear constraint solver for molecular simulation. *J. Chem. Theory Comput.* **2008**, *4*, 116−122.
(87) Berendsen, H. J.; Postma, J. P.; Van Gunsteren, W. F.; Dinola, A.; Haak, J. R. Molecular dynamics with coupling to an external bath. *J. Chem. Phys.* **1984**, *81*, 3684−3690.
(88) Bussi, G.; Donadio, D.; Parrinello, M. Canonical sampling through velocity rescaling. *J. Chem. Phys.* **2007**, *126*, 014101.
(89) Abraham, M. J.; Murtola, T.; Schulz, R.; Páll, S.; Smith, J. C.; Hess, B.; Lindahl, E. Gromacs: High performance molecular simulations through multi-level parallelism from laptops to supercomputers. *SoftwareX* **2015**, *1−2*, 19−25.
(90) Van Der Spoel, D.; Lindahl, E.; Hess, B.; Groenhof, G.; Mark, A. E.; Berendsen, H. J. GROMACS: Fast, flexible, and free. *J. Comput. Chem.* **2005**, *26*, 1701−1718.
(91) Tribello, G. A.; Bonomi, M.; Branduardi, D.; Camilloni, C.; Bussi, G. PLUMED 2: New feathers for an old bird. *Comput. Phys. Commun.* **2014**, *185*, 604−613.
(92) Matsumoto, M. Relevance of hydrogen bond definitions in liquid water. *J. Chem. Phys.* **2007**, *126*, 054503.

NOTE ADDED AFTER ASAP PUBLICATION

This paper was published ASAP on December 8, 2020, with errors in Figures 2, 4, and 6. The corrected version was reposted on December 10, 2020.

https://dx.doi.org/10.1021/acs.cgd.0c01257
Cryst. Growth Des. XXXX, XXX, XXX−XXX